biomolecules

MDPI

Article

A Series of PSMA-Targeted Near-Infrared Fluorescent Imaging Agents

Ying Chen, Il Minn, Steven P. Rowe, Alla Lisok, Samit Chatterjee, Mary Brummet, Sangeeta Ray Banerjee, Ronnie C. Mease and Martin G. Pomper *

The Russell H. Morgan Department of Radiology and Radiological Science, Johns Hopkins University School of Medicine, Baltimore, MD 21287, USA; ychen95jhmi@gmail.com (Y.C.); iminn1@jhmi.edu (I.M.); srowe8@jhmi.edu (S.P.R.); alisok1@jhmi.edu (A.L.); samitchat@gmail.com (S.C.); mbrummet@jhmi.edu (M.B.); sray9@jhmi.edu (S.R.B.); rmease1@jhmi.edu (R.C.M.)
* Correspondence: mpomper@jhmi.edu

Abstract: We have synthesized a series of 10 new, PSMA-targeted, near-infrared imaging agents intended for use in vivo for fluorescence-guided surgery (FGS). Compounds were synthesized from the commercially available amine-reactive active NHS ester of DyLight800. We altered the linker between the PSMA-targeting urea moiety and the fluorophore with a view to improve the pharmacokinetics. Chemical yields for the conjugates ranged from 51% to 86%. The K_i values ranged from 0.10 to 2.19 nM. Inclusion of an *N*-bromobenzyl substituent at the ε-amino group of lysine enhanced PSMA$^+$ PIP tumor uptake, as did hydrophilic substituents within the linker. The presence of a polyethylene glycol chain within the linker markedly decreased renal uptake. In particular, DyLight800-**10** demonstrated high specific uptake relative to background signal within kidney, confirmed by immunohistochemistry. These compounds may be useful for FGS in prostate, renal or other PSMA-expressing cancers.

Keywords: NIRF; molecular imaging; fluorescence-guided surgery; prostate-specific membrane antigen; DyLight800

Citation: Chen, Y.; Minn, I.; Rowe, S.P.; Lisok, A.; Chatterjee, S.; Brummet, M.; Banerjee, S.R.; Mease, R.C.; Pomper, M.G. A Series of PSMA-Targeted Near-Infrared Fluorescent Imaging Agents. *Biomolecules* **2022**, *12*, 405. https://doi.org/10.3390/biom12030405

Academic Editor: Albert J. Sinusas

Received: 10 January 2022
Accepted: 23 February 2022
Published: 5 March 2022

1. Introduction

As surgeons use robot-assisted laparoscopy in more operations and for an increasing number of indications, they are less likely to palpate the tumor and surgical bed to determine the extent of their resection. Accordingly, they must increasingly rely on visual inspection, which real-time fluorescence imaging can enhance by helping to avoid leaving behind a positive margin [1]. This is particularly true in the case of cancers curable only through surgery, such as colorectal cancer [2]. Advances in optical imaging instrumentation and molecular imaging agents are promoting the increased use of intraoperative, near-infrared (NIR) fluorescence imaging to help improve outcomes [3,4]. Most clinical studies employing fluorescence-guided surgery (FGS) involve the use of non-targeted protoporphyrins, such as 5-aminolevulinic acid, or cyanine dyes, such as indocyanine green, with quantum yields suitable for imaging in vivo to depths of between 0.5 and 1 cm [5,6]. However, there are a variety of available tumor-targeting moieties to which one may attach NIR dyes to confer a measure of specificity, including small molecules, peptides, proteins, antibodies, aptamers and nanobodies, among others [2,7]. One may also confer specificity of optical imaging agents through pharmacokinetic optimization in a structure-inherent targeting strategy, as recently shown for a small series of squaraine dyes [8]. The goal in designing such agents is to have one that will enable high tumor-to-background ratios at a convenient time after administration, usually within 12–24 h, for sensitive, real-time FGS.

Others and we have developed targeted NIR agents to enable specific evaluation of nerves, vascular structures within tumors, and tumor epithelium [9–13]. Regarding the last, the prostate-specific membrane antigen (PSMA) has received considerable attention as an

optical imaging target because of its abundant expression on the surface of most prostate cancer cells and the synthetic accessibility of fluorescent conjugates of urea-based PSMA-binding affinity agents [13–18]. A PSMA-targeted NIR agent could be useful toward the end of a prostatectomy to help ensure a negative surgical margin. PSMA is also expressed in the neovascular endothelium of most solid tumors, such as lung, colon, pancreatic, renal carcinoma, and melanoma, but not in normal vasculature [19,20], so it might be a useful target in surgical guidance during the resection of non-prostate tumors as well.

We have previously tested our initial PSMA-targeted NIR agent, YC-27, which bears the IRDye 800CW fluorophore, in xenograft-bearing mice and showed that it was useful in preventing recurrence in the surgical margin [21]. We have also coupled it with concurrent NIR laser excitation and ultrasound to delineate tumors by photoacoustic imaging [22]. However, YC-27 may not represent an optimized structure with respect to pharmacokinetics or properties of the fluorophore. Because of its commercial availability and putatively higher fluorescence intensity and photostability [23], we switched to the DyLight800 fluorophore and altered the structure of the linker between the fluorophore and the PSMA-targeting moiety in a series of compounds to optimize performance, i.e., tumor visualization in vivo at 24 h post-injection. Our ultimate goal is to have an imaging agent with an optimized fluorophore and pharmacokinetics for real-time surgical guidance in a field that contains PSMA-expressing tissues.

2. Materials and Methods

2.1. Chemistry

General Methods. All chemicals and solvents were purchased from either Sigma-Aldrich (Milwaukee, WI) or Fisher Scientific (Pittsburgh, PA, USA). Boc-15-amino-4,7,10,13-tetraoxapentadecanoic acid and H-Lys(Boc)-Ot-Bu.HCl were purchased from Chem-Impex International (Wood Dale, IL, USA). *t*-Boc-*N*-amido-PEG_8-acid was purchased from Broad-Pharm, Inc. (San Diego, CA, USA). The *N*-hydroxysuccinimide (NHS) ester of DyLight800 was purchased from Thermo Fisher Scientific (Rockford, IL, USA). Care was taken to limit the exposure of DyLight800-NHS and DyLight800-urea conjugates **1**–**10** from light. ^{1}H NMR spectra were recorded on a Bruker Ultrashield 500 MHz spectrometer. ESI mass spectra were obtained on a Bruker Esquire 3000 plus system. (Billerica, MA, USA). High-performance liquid chromatography (HPLC) purifications were performed on a Varian Prostar System (Varian Medical Systems, Palo Alto, CA, USA).

DyLight800-**1**: To the trifluoroacetate salt of (*S*)-5-carboxy-5-(3-((*S*)-1,3-dicarboxypropyl) ureido)pentan-1-amine, **1** [24] (0.5 mg, 1.2 µmol) in DMSO (0.1 mL), *N*,*N*-diisopropylethylamine (0.010 mL, 57.4 µmol) was added, followed by the NHS ester of DyLight800 (0.3 mg, 0.29 µmol). After 1 h at room temperature, the stirred reaction mixture was purified by HPLC (column, Phenomenex Luna C18, 10 µ, 250 × 4.6 mm; mobile phase, A = 0.1% TFA in H_2O, B = 0.1% TFA in CH_3CN; linear gradient, 0 min = 5% B, 5 min = 5% B, 45 min = 100% B; flow rate, 1 mL/min) to afford 0.3 mg (87%) of DyLight800-**1**. ESI-Mass calculated for $C_{57}H_{69}N_5O_{18}S_3^{2-}$ $[M\text{-}2H]^{2-}$ 603.7 found 603.6.

DyLight800-**2**: To a solution of (*S*)-*N*-(4-bromobenzyl)-5-carboxy-5-(3-((*S*)-1,3-dicarboxypropyl) ureido)pentan-1-amine **2** *(20)* (0.5 mg, 1.0 µmol) in DMSO (0.1 mL), *N*,*N*-diisopropylethylamine (0.005 mL, 28.7 µmol) was added, followed by the NHS ester of DyLight800 (0.3 mg, 0.29 µmol). After stirring overnight at room temperature, the reaction mixture was purified by HPLC (column, Phenomenex Luna C18, 10 µ, 250 × 4.6 mm; mobile phase, H_2O/CH_3CN/TFA = 67/33/0.1; flow rate, 1 mL/min) to afford 0.2 mg (51%) of DyLight800-**2**. ESI-Mass calculated for $C_{64}H_{74}BrN_5O_{18}S_3^{2-}$ $[M\text{-}2H]^{2-}$ 687.7 found 687.5.

DyLight800-**3**: To the trifluoroacetate salt of (3*S*,7*S*,22*S*)-1,3,7,22-tetracarboxy-5,13,20-trioxo-4,6,12,21-tetraazahexacosan-26-amine **3** (*9*), (0.5 mg, 0.7 µmol) in DMSO (0.1 mL), *N*,*N*-diisopropylethylamine (0.010 mL, 57.4 µmol) was added, followed by the NHS ester of DyLight800 (0.3 mg, 0.29 µmol). After 1 h at room temperature, the stirred reaction mixture was purified by HPLC (column, Phenomenex Luna C18, 10 µ, 250 × 4.6 mm; mobile phase, A = 0.1% TFA in H_2O, B = 0.1% TFA in CH_3CN; linear gradient, 0 min = 5% B, 5 min = 5%

B, 45 min = 100% B; flow rate,1 mL/min) to afford 0.3 mg (70%) of DyLight800-**3**. ESI-Mass calculated for $C_{71}H_{94}N_7O_{22}S_3^-$ $[M-H]^-$ 1492.6 found 1492.4.

(3*S*,7*S*)-12-(4-Bromobenzyl)-1,3,7-tricarboxy-5,13,20-trioxo-4,6,12,21-tetraazahexacosan-26-aminium trifluoroacetate, **4**. To a solution of (*S*)-*N*-(4-bromobenzyl)-6-(tert-butoxy)-5-(3-((*S*)-1,5-di-tert-butoxy-1,5-dioxopentan-2-yl)ureido)-6-oxohexan-1-amine, **12** [25] (0.066 g, 0.1 mmol) in CH_2Cl_2 (4 mL), triethylamine (0.05 mL, 0.36 mmol) was added, followed by (*S*)-2,5-dioxopyrrolidin-1-yl 8-((1-(*tert*-butoxy)-6-((*tert*-butoxycarbonyl)amino)-1-oxohexan-2-yl)amino)-8-oxooctanoate, **11** (0.060 g, 0.11 mmol). After stirring overnight at room temperature, the solvent was evaporated and a solution of TFA/H_2O (95:5, 0.3 mL) was added. The mixture was kept at room temperature for 1 h, then purified by HPLC (column, Phenomenex Luna C18, 10 µ, 250 × 10 mm; mobile phase, A = 0.1% TFA in H_2O, B = 0.1% TFA in CH_3CN; linear gradient, 0 min = 5% B, 5 min = 5% B, 25 min = 100% B; flow rate, 4 mL/min) to afford 0.048 g (55%) of **4**. ^{1}H NMR (500 MHz, D_2O, compound exists as a mixture of rotamers) δ 7.40–7.45 (m, 2H), 7.04 (m, 2H), 4.44–4.51 (m, 2H), 4.19–4.25 (m, 2H), 4.08 (m, 1H), 3.26 (m, 2H), 2.91 (m, 2H), 2.38–2.42 (m, 3H), 2.17–2.25 (m, 3H), 2.08–2.10 (m, 1H), 1.81–1.89 (m, 2H), 1.37–1.68 (m, 13H), 1.25 (m,4H). 1.14 (m, 2H). ESI-Mass calculated for $C_{33}H_{51}BrN_5O_{11}^+$ $[M + H]^+$ 772.3 found 772.2.

DyLight800-**4**: To a solution of **4** (0.5 mg, 0.57 µmol) in DMSO (0.1 mL), *N*,*N*-diisopropylethylamine (0.010 mL, 57.4 µmol) was added, followed by the NHS ester of DyLight800 (0.5 mg, 0.48 µmol). After stirring for 1 h at room temperature, the reaction mixture was purified by HPLC (column, Phenomenex Luna C18, 10 µ, 250 × 4.6 mm; mobile phase, A = 0.1% TFA in H_2O, B = 0.1% TFA in CH_3CN; linear gradient, 0 min = 5% B, 5 min = 5% B, 45 min = 100% B; flow rate, 1 mL/min) to afford 0.5 mg (63%) of DyLight800-**4**. ESI-Mass calculated for $C_{78}H_{98}BrN_7O_{22}S_3^{2-}$ $[M-2H]^{2-}$ 829.9 found 830.5.

(3*S*,7*S*)-1,3,7-Tricarboxy-5,13,20-trioxo-4,6,12,21-tetraazahexacosan-26-aminium trifluoroacetate **5**: To the formate of (*S*)-6-(*tert*-butoxy)-5-(3-((*S*)-1,5-di-*tert*-butoxy-1,5-dioxopentan-2-yl)ureido)-6-oxohexan-1-amine, **15** (0.027 g, 0.05 mmol) [24] in CH_2Cl_2 (2 mL), triethylamine (0.02 mL, 0.14 mmol) was added, followed by 2,5-dioxopyrrolidin-1-yl 8-((5-((*tert*-butoxycarbonyl)amino)pentyl)amino)-8-oxooctanoate,**13** (0.023 g, 0.05 mmol). After stirring at room temperature for 2 h, the solvent was evaporated and the residue was purified by a silica gel column (5% MeOH in CH_2Cl_2) to give the protected intermediate (0.037 g, 0.044mmol) 88%). ESI-Mass calculated for $C_{42}H_{78}N_5O_{11}$ $[M + H]^+$ 828.6 found 828.6. To this, a solution of TFA/H_2O (95:5, 0.3 mL) was added. The mixture was stirred at ambient temperature for 2 h, then purified on a Sep-Pak Vac 12 cc syringe column (Waters) using a gradient of water to acetonitrile/water 5:5 (*v*:*v*) to give compound **5** (0.023 g, 78%). ^{1}H NMR (500 MHz, D_2O/CD_3CN = 2:1) δ 3.97–4.02 (m, 2H), 3.05 (m, 4H), 2.83–2.86 (m, 2H), 2.31 (m, 2H), 2.09 (m, 4H), 1.79 (m, 1H), 1.66 (m, 1H), 1.40–1.56 (m, 12H), 1.19–1.28 (m, 8H). ESI-Mass calculated for $C_{25}H_{46}N_5O_9^+$ $[M + H]^+$ 560.3 found 560.3.

DyLight800-**5**: To a solution of compound 5 (0.5 mg, 0.74 µmol) in DMSO (0.1 mL), *N*,*N*-diisopropylethylamine (0.010 mL, 57.4 µmol) was added, followed by the NHS ester of DyLight800 (0.3 mg, 0.29 µmol). After stirring 2 h at room temperature, the reaction mixture was purified by HPLC (column, Phenomenex Luna C18, 10 µ, 250 × 4.6 mm; mobile phase, A = 0.1% TFA in H_2O, B = 0.1% TFA in CH_3CN; linear gradient, 0 min = 5% B, 5 min = 5% B, 25 min = 100% B; flow rate, 1 mL/min) to afford 0.3 mg (72%) of DyLight800-**5**. ESI-Mass calculated for $C_{70}H_{93}N_7O_{20}S_3^{2-}$ $[M-2H]^{2-}$, 723.8, found 723.6.

(3*S*,7*S*)-12-(4-Bromobenzyl)-1,3,7-tricarboxy-5,13,20-trioxo-4,6,12,21-tetraazahexacosan-26-aminium trifluoroacetate, **6**: To a solution of compound **12** (0.016 g, 0.024 mmol) in CH_2Cl_2 (2 mL), triethylamine (0.01 mL, 0.072 mmol) was added, followed by **13** (0.011 g, 0.024 mmol). After stirring at room temperature for 2 h, the solvent was evaporated and the residual was purified by HPLC (column, Phenomenex Luna C18, 10 µ, 250 × 10 mm; mobile phase, A = 0.1% TFA in H_2O, B = 0.1% TFA in CH_3CN; linear gradient, 0 min = 40% B, 5 min = 40% B, 25 min = 100% B; flow rate, 4 mL/min) to give 0.013 g (54%) of the protected intermediate. ESI-Mass calculated for $C_{49}H_{83}BrN_5O_{11}$ $[M + H]^+$ 996.5 found 996.4. To the protected intermediate, a solution of TFA/H_2O (95:5, 0.3 mL) was added. The

mixture was kept at ambient temperature for 2 h, then purified on a Sep-Pak Vac 12 cc syringe column (Waters) using a gradient of water to acetonitrile/water of 5:5 (*v*:*v*) to give compound **6** (0.008 g, 73%). ^{1}H NMR (500 MHz, D_2O/CD_3CN = 1:1, compound exists as a mixture of rotamers) δ 7.43–7.49 (m, 2H), 7.08 (m, 2H), 4.43–4.49 (m, 2H), 4.02–4.08 (m, 2H), 3.18–3.26 (m, 2H), 3.04–3.08 (m, 2H), 2.82–2.85 (m, 2H), 2.23–2.36 (m, 4H), 2.08–2.11 (m, 2H), 1.79–1.82 (m, 1H), 1.66 (m, 1H),1.49–1.58 (m, 12H), 1.13–1.26 (m, 8H). ESI-Mass calculated for $C_{32}H_{51}BrN_5O_9^+$ $[M + H]^+$ 728.3 found 728.2.

DyLight800-**6**: To a solution of compound 6 (0.5 mg, 0.59 μmol) in DMSO (0.1 mL), *N*,*N*-diisopropylethylamine (0.010 mL, 57.4 μmol) was added, followed by the NHS ester of DyLight800 (0.3 mg, 0.29 μmol). After stirring 2 h at room temperature, the reaction mixture was purified by HPLC (column, Phenomenex Luna C18, 10 μ, 250 × 4.6 mm; mobile phase, A = 0.1% TFA in H_2O, B = 0.1% TFA in CH_3CN; linear gradient, 0 min = 5% B, 5 min = 5% B, 25 min = 100% B; flow rate, 1 mL/min) to afford 0.4 mg (86%) of DyLight800-**6**. ESI-Mass calculated for $C_{77}H_{98}BrN_7O_{20}S_3^{2-}$ $[M-2H]^{2-}$, 807.8, found 808.6.

(21*S*,25*S*)-21,25,27-Tricarboxy-15,23-dioxo-3,6,9,12-tetraoxa-16,22,24-triazaheptacosan-1-aminium trifluoroacetate, **7**: To a solution of 15 (0.053 g, 0.1 mmol) in CH_2Cl_2 (2 mL), triethylamine (0.027 mL, 0.2 mmol) was added, followed by 2,5-dioxopyrrolidin-1-yl 2,2-dimethyl-4-oxo-3,8,11,14,17-pentaoxa-5-azaicosan-20-oate, **17** (0.046 g, 0.1 mmol). After stirring at room temperature for 2 h, the solvent was evaporated and the residue was purified by a silica gel column (5% MeOH in CH_2Cl_2) to give the protected intermediate (0.051 g, 61%). ESI-Mass calculated for $C_{40}H_{74}N_4O_{14}Na$ $[M + Na]^+$ 857.5 found 857.5. To the protected intermediate, a solution of TFA/H_2O (95:5, 0.2 mL) was added. The mixture was stirred at ambient temperature for 2 h, then purified using a Sep-Pak Vac 12 cc syringe column (Waters) using a gradient of 100% water to acetonitrile/water 3:7 (*v*:*v*). Product fractions were collected and lyophilized to give compound **7** (0.032 g, 79%). ^{1}H NMR (500 MHz, D_2O) δ 4.20 (m, 1H), 4.12 (m, 1H), 3.76 (m, 4H), 3.65–3.70 (m, 12H), 3.17–3.20 (m, 4H), 2.46–2.50 (m, 4H), 2.12–2.15 (m, 1H), 1.92–1.98 (m, 1H), 1.78–1.83 (m, 1H), 1.64–1.72 (m, 1H), 1.49–1.55 (m, 2H), 1.37–1.41 (m, 2H). ESI-Mass calculated for $C_{23}H_{43}N_4O_{12}^+$ $[M + H]^+$ 567.3 found 567.2.

DyLight800-**7**: To a solution of compound **7** (0.3 mg, 0.45 μmol) in DMSO (0.1 mL), *N*,*N*-diisopropylethylamine (0.010 mL, 57.4 μmol) was added, followed by the NHS ester of DyLight800 (0.3 mg, 0.29 μmol). After stirring for 2 h at room temperature, the reaction mixture was purified by HPLC (column, Phenomenex Luna C18, 10 μ, 250 × 4.6 mm; mobile phase, A = 0.1% TFA in H_2O, B = 0.1% TFA in CH_3CN; gradient, 0 min = 5% B, 5 min = 5% B, 45 min = 100% B; flow rate, 1 mL/min) to afford 0.3 mg (72%) of DyLight800-**7**. ESI-Mass calculated for $C_{68}H_{90}N_6O_{23}S_3^{2-}$ $[M-2H]^{2-}$ 727.3 found 727.1.

(21*S*,25*S*)-16-(4-Bromobenzyl)-21,25,27-tricarboxy-15,23-dioxo-3,6,9,12-tetraoxa-16,22,24-triazaheptacosan-1-aminium trifluoroacetate, **8**: To a solution of compound **12** (0.066 g, 0.1 mmol) in CH_2Cl_2 (2 mL), triethylamine (0.027 mL, 0.2 mmol) was added, followed by 2,5-dioxopyrrolidin-1-yl 2,2-dimethyl-4-oxo-3,8,11,14,17-pentaoxa-5-azaicosan-20-oate, **17** (0.046 g, 0.1 mmol). After stirring for 2 h at room temperature, the solvent was evaporated, and the residue was purified by a silica gel column (5% MeOH in CH_2Cl_2) to give the protected intermediate (0.082 g, 81%) ESI-Mass calculated for $C_{47}H_{79}BrN_4O_{14}Na^+$ $[M + Na]^+$ 1025.5 found 1025.3. To the protected intermediate, a solution of TFA/H_2O (95:5, 0.2 mL) was added. The mixture was kept at an ambient temperature for 2 h, and the solvent was evaporated and the residue purified on a Sep-Pak Vac 12 cc syringe column (Waters) using a gradient of 100% water to acetonitrile/water 1:1 (*v*:*v*). The fractions were collected and lyophilized to give compound **8** (0.056 g, 67%). ^{1}H NMR (500 MHz, D_2O, compound exists as a mixture of rotamers) δ 7.49–7.55 (m, 2H), 7.12–7.15 (m, 2H), 4.52–4.61 (m, 2H), 4.10 (m, 1H), 4.03 (m, 1H), 3.68–3.80 (m, 4H), 3.54–3.64 (m, 12H), 3.32–3.38 (m, 2H), 3.13–3.15 (m, 2H), 2.62–2.76 (m, 2H), 2.37–2.40 (m, 2H), 2.04–2.08 (m, 1H), 1.86–1.89 (m, 1H), 1.67–1.73 (m, 1H), 1.51–1.61 (m, 3H), 1.26–1.30 (m, 2H). ESI-Mass calculated for $C_{30}H_{48}BrN_4O_{12}^+$ $[M + H]^+$ 735.2 found 735.2.

DyLight800-**8**: To a solution of compound **8** (0.5 mg, 0.60 µmol) in DMSO (0.1 mL), *N*,*N*-diisopropylethylamine (0.010 mL, 57.4 µmol) was added, followed by the NHS ester of DyLight800 (0.3 mg, 0.29 µmol). After stirring for 2 h at room temperature, the reaction mixture was purified by HPLC (column, Phenomenex Luna C18, 10 µ, 250 × 4.6 mm; mobile phase, A = 0.1% TFA in H_2O, B = 0.1% TFA in CH_3CN; gradient, 0 min = 5% B, 5 min = 5% B, 45 min = 100% B; flow rate, 1 mL/min) to afford 0.3 mg (65%) of DyLight800-**8**. ESI-Mass calculated for $C_{75}H_{95}BrN_6O_{23}S_3{}^{2-}$ $[M\text{-}2H]^{2-}$ 811.2 found 811.0.

2,5-Dioxopyrrolidin-1-yl 2,2-dimethyl-4-oxo-3,8,11,14,17,20,23,26,29-nonaoxa-5-azadotriacontan-32-oate, **20**: To a solution of *t*-Boc-*N*-amido-PEG_8-acid (0.25 g, 0.46 mmol) and *N*-hydroxysuccinimide (0.053 g, 0.046 mmol) in CH_2Cl_2 (4 mL), dicyclohexylcarbodiimide (0.1 g, 0.048 mmol) was added. After stirring at room temperature overnight, the mixture was filtered, and the filtrate was evaporated to give compound **20**. ESI-Mass calculated for $C_{28}H_{50}N_2O_{14}Na$ $[M + Na]^+$ 661.3 found 661.3.

(33*S*,37*S*)-33,37,39-Tricarboxy-27,35-dioxo-3,6,9,12,15,18,21,24-octaoxa-28,34,36-triazanonatriacontan-1-aminium trifluoroacetate **9**: To a solution of the formate salt of **15** (0.053 g, 0.1 mmol) in CH_2Cl_2 (2 mL), triethylamine (0.027 mL, 0.2 mmol) was added, followed by 2,5-dioxopyrrolidin-1-yl 2,2-dimethyl-4-oxo-3,8,11,14,17,20,23,26,29-nonaoxa-5-azadotriacontan-32-oate, **20** (0.070 g, 0.11 mmol). After 2 h of stirring at room temperature, the solvent was evaporated, and the residual was purified by a silica gel column (5% MeOH in CH_2Cl_2) to give the protected intermediate (0.076 g, 76%). A solution of TFA/H_2O (95:5, 0.2 mL) was added to the protected intermediate (0.060 g, 0.059 mmol). The mixture was kept at an ambient temperature for 2 h, then purified by Sep-Pak Vac 12 cc (Waters) using a gradient of water to acetonitrile/water of 3:7 (*v*:*v*). The fractions were collected and lyophilized to give compound **9** (0.036 g, 72%). ^{1}H NMR (500 MHz, D_2O) δ 4.12 (m, 1H), 4.07 (m, 1H), 3.76 (m, 4H), 3.65–3.70 (m, 28H), 3.17–3.20 (m, 4H), 2.48–2.50 (m, 2H), 2.41–2.44 (m, 2H), 2.06–2.10 (m, 1H), 1.88–1.92 (m, 1H), 1.76–1.79 (m, 1H), 1.65–1.69 (m, 1H), 1.49–1.53 (m, 2H), 1.35–1.38 (m, 2H). ESI-Mass calculated for $C_{31}H_{59}N_4O_{16}{}^+$ $[M + H]^+$ 743.4 found 743.3.

DyLight800-**9**: To a solution of compound **9** (0.5 mg, 0.60 µmol) in DMSO (0.1 mL), *N*,*N*-diisopropylethylamine (0.010 mL, 57.4 µmol) was added, followed by the NHS ester of DyLight800 (0.3 mg, 0.29 µmol). After stirring for 2 h at room temperature, the reaction mixture was purified by HPLC (column, Phenomenex Luna C18, 10 µ, 250 × 4.6 mm; mobile phase, A = 0.1% TFA in H_2O, B = 0.1% TFA in CH_3CN; gradient, 0 min = 5% B, 5 min = 5% B, 45 min = 100% B; flow rate, 1 mL/min) to afford 0.4 mg (86%) of DyLight800-**9**. ESI-Mass calculated for $C_{76}H_{106}N_6O_{27}S_3{}^{2-}$ $[M\text{-}2H]^{2-}$ 815.3 found 815.1.

(33S,37*S*)-28-(4-Bromobenzyl)-33,37,39-tricarboxy-27,35-dioxo-3,6,9,12,15,18,21,24-octaoxa-28,34,36-triazanonatriacontan-1-aminium trifluoroacetate **10**: To a solution of compound 12 (0.066 g, 0.1 mmol) in CH_2Cl_2 (3 mL), triethylamine (0.027 mL, 0.2 mmol) was added, followed by 2,5-dioxopyrrolidin-1-yl 2,2-dimethyl-4-oxo-3,8,11,14,17,20,23,26,29-nonaoxa-5-azadotriacontan-32-oate, **20**, (0.070 g, 0.11 mmol). After stirring overnight at room temperature, the solvent was evaporated, and the residue was purified on a silica gel column (5% MeOH in CH_2Cl_2) to give the protected intermediate (0.094 g, 79%). To the protected intermediate (0.07 g, 0.059 mmol), a solution of TFA/H_2O (95:5, 0.2 mL) was added. The mixture was kept at ambient temperature for 2 h, then purified by HPLC (column: Phenomenex Luna C18, 10 µ, 250 × 10 mm; mobile phase, A = 100% water + 0.1%TFA, B = 100% acetonitrile + 0.1% TFA, Linear Gradient: 0 min 100%A, 25 min 100%B; flow rate, 4 mL/min) to give compound 10 (0.031g, 52%). ^{1}H NMR (500 MHz, D_2O, compound exists as a mixture of rotamers) δ 7.49–7.53 (m, 2H), 7.12–7.16 (m, 2H), 4.52–4.61 (m, 2H), 4.21 (m, 1H), 4.10 (m, 1H), 3.71–3.80 (m, 4H), 3.54–3.66 (m, 28H), 3.32–3.38 (m, 2H), 3.15–3.16 (m, 2H), 2.63–2.78 (m, 2H), 2.44–2.47 (m, 2H), 2.09–2.15 (m, 1H), 1.88–1.96 (m, 1H), 1.71–1.77 (m, 1H), 1.50–1.64 (m, 3H), 1.28–1.30 (m, 2H). ESI-Mass calculated for $C_{38}H_{64}BrN_4O_{16}{}^+$ $[M + H]^+$ 912.9 found 913.3.

DyLight800-**10**: To a solution of compound **10** (0.5 mg, 0.50 µmol) in DMSO (0.1 mL), *N*,*N*-diisopropylethylamine (0.010 mL, 57.4 µmol), followed by the NHS ester of DyLight800

(0.3 mg, 0.29 μmol) was added. After stirring for 2 h at room temperature, the reaction mixture was purified by HPLC (column, Phenomenex Luna C18, 10 μ, 250 × 4.6 mm; mobile phase, A = 0.1% TFA in H_2O, B = 0.1% TFA in CH_3CN; gradient, 0 min = 5% B, 5 min = 5% B, 45 min = 100% B; flow rate, 1 mL/min) to afford 0.3 mg (58%) of DyLight800-**10**. ESI-Mass calculated for $C_{83}H_{111}BrN_6O_{27}S_3^{2-}$ $[M\text{-}2H]^{2-}$ 899.3 found 899.1.

Synthetic details for the linkers used in compounds **4**–**10** are presented in the Supplemental Materials.

2.2. NAALADase Assay

Cell lysates of LNCaP cell extracts were incubated with PSMA-targeted imaging agents (0.01 nM–100 μM) in the presence of 4 μM NAAG at 37 °C for 2 h. The amount of released glutamate from NAAG was measured by incubating with a working solution of the Amplex Red glutamic acid kit (Molecular Probes Inc., Eugene, OR, USA) at 37 °C for 60 min. Fluorescence was determined by reading with the Cytation 5 Cell Imaging Multi-Mode Reader (BioTek, Winooski, VT, USA) with excitation at 545 nm and emission at 590 nm [26]. Inhibition curves were determined using semi-log plots, and IC_{50} values were determined as the concentration at which enzymatic activity was inhibited by 50%. Assays were performed in triplicate, with the entire inhibition study being repeated at least once to confirm the affinity and mode of inhibition. Enzyme inhibitory constants (K_i values) were generated using the Cheng–Prusoff conversion [27]. Data analysis was performed using GraphPad Prism version 9 for Windows (GraphPad Software, San Diego, CA, USA).

2.3. Cell Lines and Tumor Models

$PSMA^+$ PC3 PIP and $PSMA^-$ PC3 flu cell lines were originally obtained from Dr. Warren Heston (Cleveland Clinic). Cells were grown to 80–90% confluence in a single passage before trypsinization and formulation in Hank's balanced salt solution (HBSS, Sigma, St. Louis, MO, USA) for implantation into mice. PC3-ML-PSMA [28] cells maintained in RPMI1640 supplemented with 10% FBS and 1× Pen/Strep. Animal studies were carried out in compliance with guidelines related to the conduct of animal experiments of the Johns Hopkins Animal Care and Use Committee. For optical imaging studies and ex vivo biodistribution, male NOD-SCID mice (Johns Hopkins University, in-house colony) were implanted subcutaneously with 1×10^6 $PSMA^+$ PC3 PIP and $PSMA^-$ PC3 flu cells in opposite flanks. Mice were imaged when the tumor xenografts reached 3–5 mm in diameter. For the metastatic model of a PSMA-expressing prostate tumor, 1×10^6 PC3-ML-PSMA cells were injected intravenously into 4 to 6-week-old NSG (NOD/Shi-scid/IL-2Rγnull) mice (Animal Resources Core, Johns Hopkins). Four weeks post-injection of the cells, animals were used for imaging.

2.4. In Vivo Imaging and Ex Vivo Biodistribution

After image acquisition at baseline (pre-injection), each mouse was injected intravenously with 1 nmol of DyLight800-urea conjugate (DyLight800-**1** to DyLight800-**10**, **3**–**4** mice per compound), and images were acquired at 1 h, 2 h, 4 h and 24 h time points using a Pearl Impulse Imager (LI-COR Biosciences, Cambridge, UK). Following the 24 h image, each mouse was sacrificed by cervical dislocation, and tumor, muscle, liver, spleen, kidneys and stomach were collected and assembled on a petri dish for image acquisition. All images were scaled to the same intensity for direct comparison.

2.5. Immunohistochemistry (IHC)

The kidney and liver were fixed in 10% formalin for 24 h and embedded in paraffin. Sectioning and H&E staining were performed by Johns Hopkins Oncology Tissue Services. For PSMA IHC, slides were stained with anti-PSMA antibody (Cat# SIR089, Dako, Santa Clara, CA, USA) with 1:2 dilution in the presence of background reducing components (Cat# S3022, Dako). Slides were then stained with anti-mouse HRP linked antibody from EnVision plus system-HRP (DAB) (Cat# K4006, Dako). Processed slides were scanned by

Johns Hopkins Oncology Tissue Services, and the images were analyzed using Aperio Image Scope software (Leica Biosystems Inc, Buffalo Grove, IL, USA).

2.6. Statistical Considerations

An unpaired *t*-test was performed to determine whether there were differences in $PSMA^+$ PC3 PIP tumor uptake and the kidney and corresponding $PSMA^-$ PC3 flu tumor for DyLight800-**1**–**10**. Statistical significance was determined to be present at $p < 0.01$. Calculations were performed using GraphPad Prism 9 (San Diego, CA, USA).

3. Results

3.1. Chemical Synthesis

General syntheses of DyLight800-**1** and -**2** (no linker) are presented in Scheme 1, while general syntheses of DyLight-**3** through -**10** (with linker) are shown in Scheme 2.

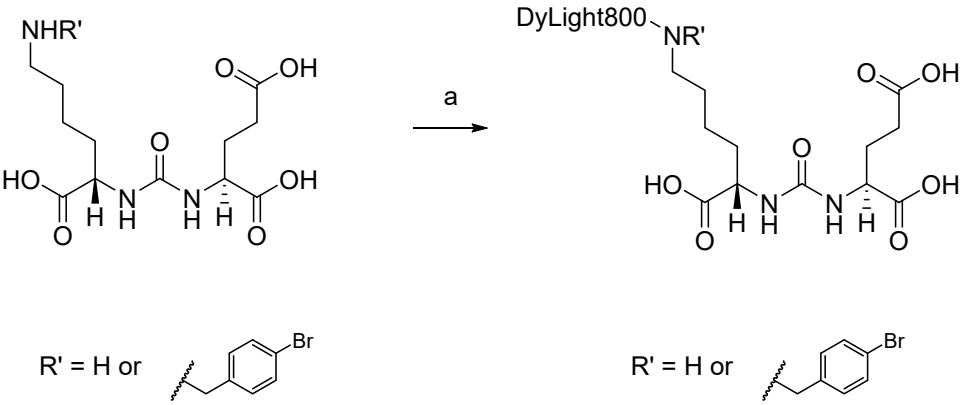

Scheme 1. General syntheses of DyLight800-**1** (R′ = H) and -**2** (no linker, R′ = *para*-BrBn).

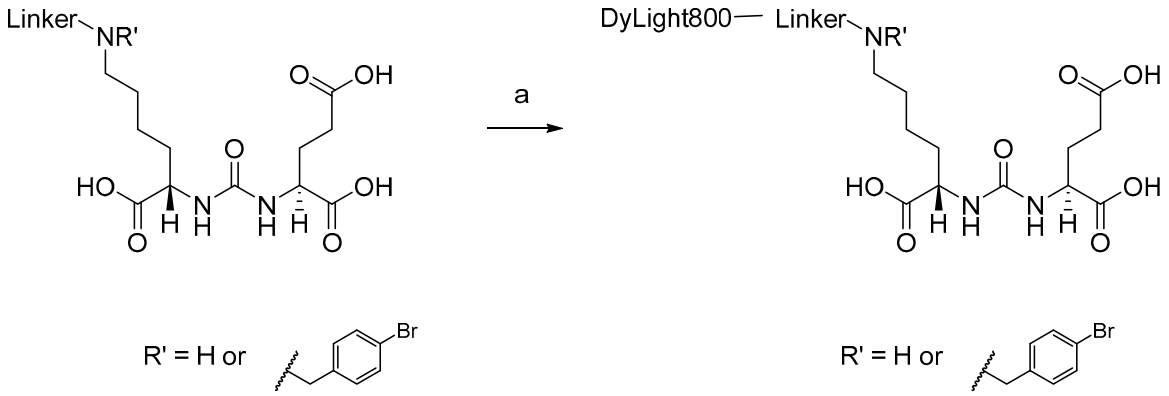

Scheme 2. General syntheses of DyLight800-**3** to -**10**. (See Figure 1 for R′ and linkers).

Commercially available amine-reactive active NHS ester of DyLight800 with principal excitation/emission wavelength at 777/794 nm was conjugated with amines **1**–**10** to produce the dye-PSMA inhibitors shown in Figure 1. The conjugation reactions were readily completed at room temperature. The chemical yields for the conjugates ranged from 51% to 86%.

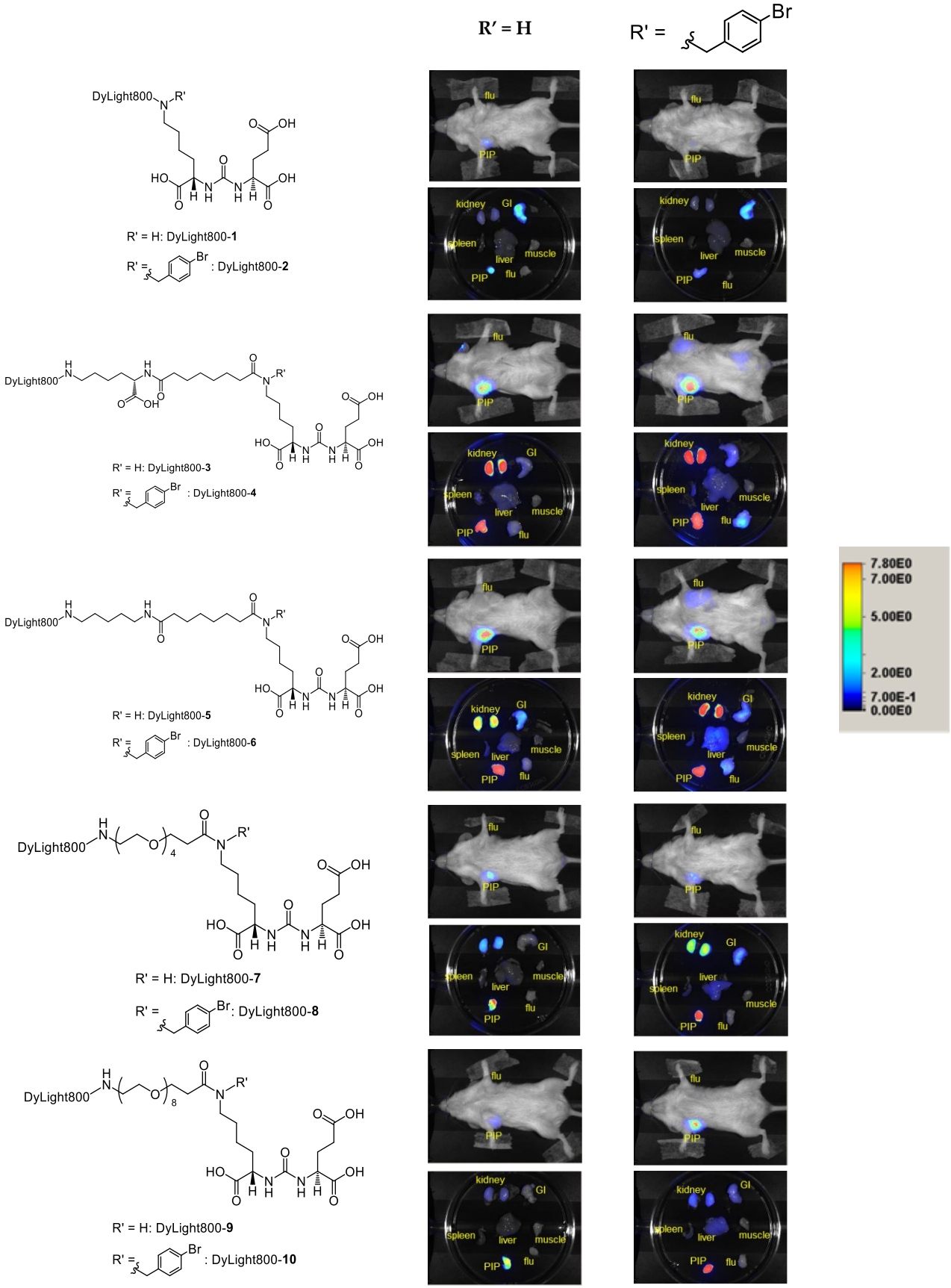

Figure 1. Whole body and excised organ imaging of mice with PSMA$^+$ PC3 PIP and PSMA- PC3 flu tumors at 24 h post-injection of 1 nmol of DyLight800-urea conjugates.

3.2. In Vitro Inhibition Assay

The K_i values were determined using a modification of the Amplex Red glutamic acid assay [26] and are presented in Table 1. The K_i values range from 0.10 to 2.19 nM, which is similar to other compounds of this class [29].

Table 1. PSMA inhibitory activities.

Compound	K_i (nM)	95% Confidence Interval of K_i
DyLight800-**1**	0.37	0.26–0.52
DyLight800-**2**	0.16	0.11–0.22
DyLight800-**3**	0.10	0.06–0.15
DyLight800-**4**	0.29	0.17–0.51
DyLight800-**5**	0.45	0.31–0.65
DyLight800-**6**	0.68	0.40–1.17
DyLight800-**7**	0.85	0.52–1.36
DyLight800-**8**	0.50	0.34–0.73
DyLight800-**9**	2.19	1.22–2.71
DyLight800-**10**	0.83	0.73–0.94

3.3. Imaging

Figure 1 shows the imaging at 24 h post-injection of 1 nmol of compound DyLight800-**1** to DyLight800-**10** in mice with PSMA$^+$ PC3 PIP and PSMA$^-$ PC3 flu tumors. All ten compounds demonstrated robust PSMA$^+$ PC3 PIP tumor uptake and little uptake in PSMA$^-$ PC3 flu tumors, indicating target selectivity in vivo. Fluorescence intensities of PIP, flu, kidney and liver are shown in Figure 2A. We found significant differences in uptake of each agent between the PSMA-expressing tumors and kidney and between these tumors and the PSMA-negative tumors according to the levels of significance indicated.

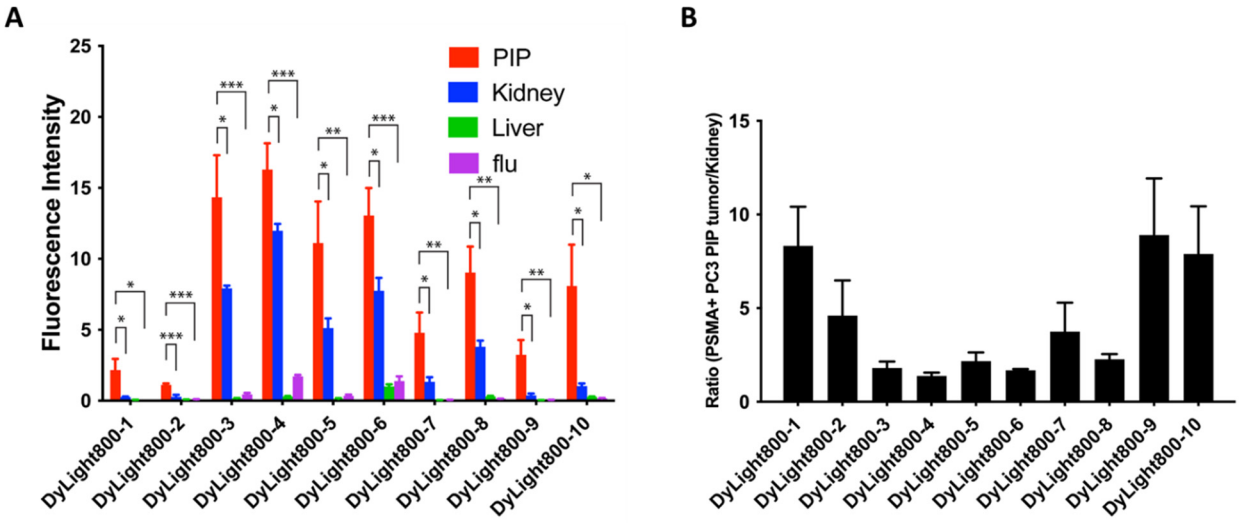

Figure 2. (**A**) Biodistribution data at 24 h postinjection from regions of interest (ROI) drawn over organs displayed in ex vivo images. Three to four animals were imaged per agent. Comparisons were made between the tumor and kidney, as well as between PSMA+ PC3 PIP tumor and kidney and between PSMA$^+$ PC3 PIP and PSMA$^-$ PC3 flu tumor. Values are represented as mean ± standard error of the mean (SEM). PIP = PSMA$^+$ PC3 PIP tumor; flu = PSMA$^-$ PC3 flu tumor. * = $p < 0.01$; ** = $p < 0.001$; *** = $p < 0.0001$. (**B**) Ratio of uptake in PSMA$^+$ PC3 PIP tumor to kidney based on the data in panel (**A**).

As noted above, the key consideration for a suitable FGS agent is tumor/background at the time of surgery. The agent must also have high absolute tumor uptake to be detectable. DyLight800-**3**, DyLight800-**4**, DyLight800-**5** and DyLight800-**6** demonstrated the highest PSMA$^+$ PIP tumor uptake. Comparing DyLight800-**7** and DyLight800-**9** with DyLight800-**8** and DyLight800-**10**, it was demonstrated that the *N*-bromobenzyl substituent significantly increased the PSMA$^+$ PIP tumor uptake. DyLight800-**1** and DyLight800-**2**, which have no linker between the dye and Lys-Glu urea, had much lower PSMA$^+$ PIP tumor uptake than other compounds with linkers, confirming the importance of the linker moiety for modifying pharmacokinetics. DyLight800-**7**, DyLight800-**8**, DyLight800-**9** and DyLight800-**10**, which have PEG_4 or PEG_8 linker had significantly less kidney uptake compared to DyLight800-**3**, DyLight800-**4**, DyLight800-**5** and DyLight800-**6**. While Dylight800-**1**, Dylight800-**9** and DyLight800-**10** showed the most favorable tumor/background, their absolute uptake levels were relatively low. Nevertheless, for renal surgery, one of them, particularly DyLight-**10**, may have the best properties (Figure 2B). DyLight800-**3** or DyLight800-**4** may be superior for prostate surgery, due to higher absolute uptake where renal uptake is of no consequence. Figure 3 shows the capacity for the dyes to identify lesions within metastatic foci of liver and kidney, while Figure 4 provides correlative histology from this experiment.

We also compared the uptake of DyLight800-**3** to that of our previously published compound YC-27 (Figure 5) [13]. Qualitatively, the uptake in tumor of DyLight800-**3** is similar to or slightly higher than that of YC-27, while renal uptake is much lower for the latter. Note that these two compounds differ only in the fluorophore, with YC-27 bearing the IRDye 800CW dye.

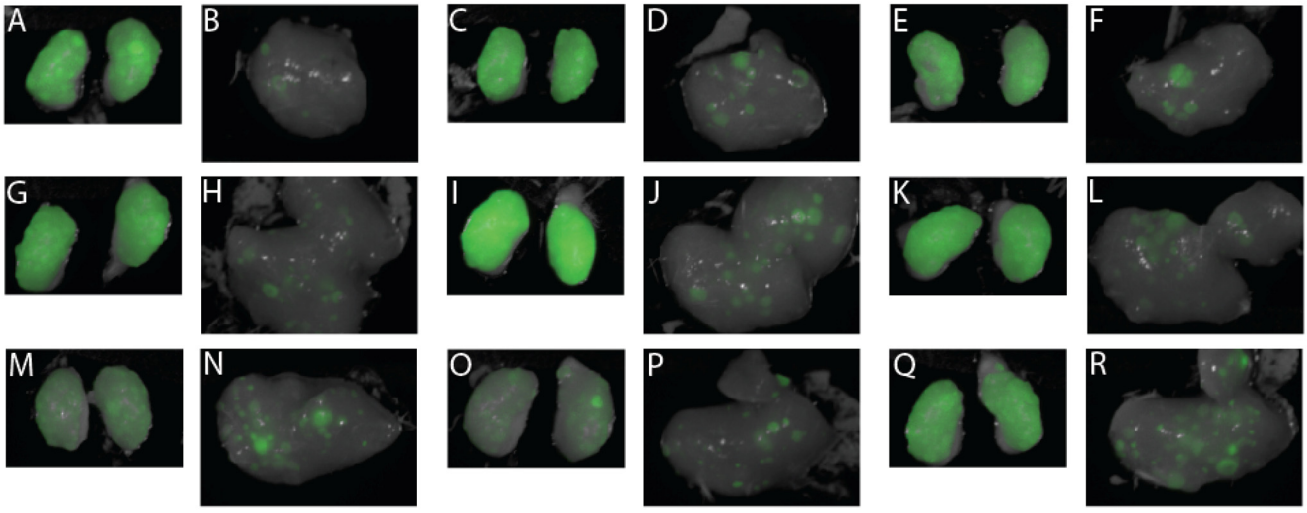

Figure 3. Selected agents successfully detected PSMA-expressing metastatic lesions in the kidney and liver. Ex vivo fluorescent images of kidney (**A**,**C**,**E**,**G**,**I**,**K**,**M**,**O**,**Q**) and liver (**B**,**D**,**F**,**H**,**J**,**L**,**N**,**P**,**R**) from mice injected with 1 nmole of compounds DyLight800-**4** (**A**–**F**), DyLight800-**6** (**G**–**L**), and DyLight800-**10** (**M**–**R**). Fluorescence intensity was optimized to maximize the contrast between tumor and kidney for each image.

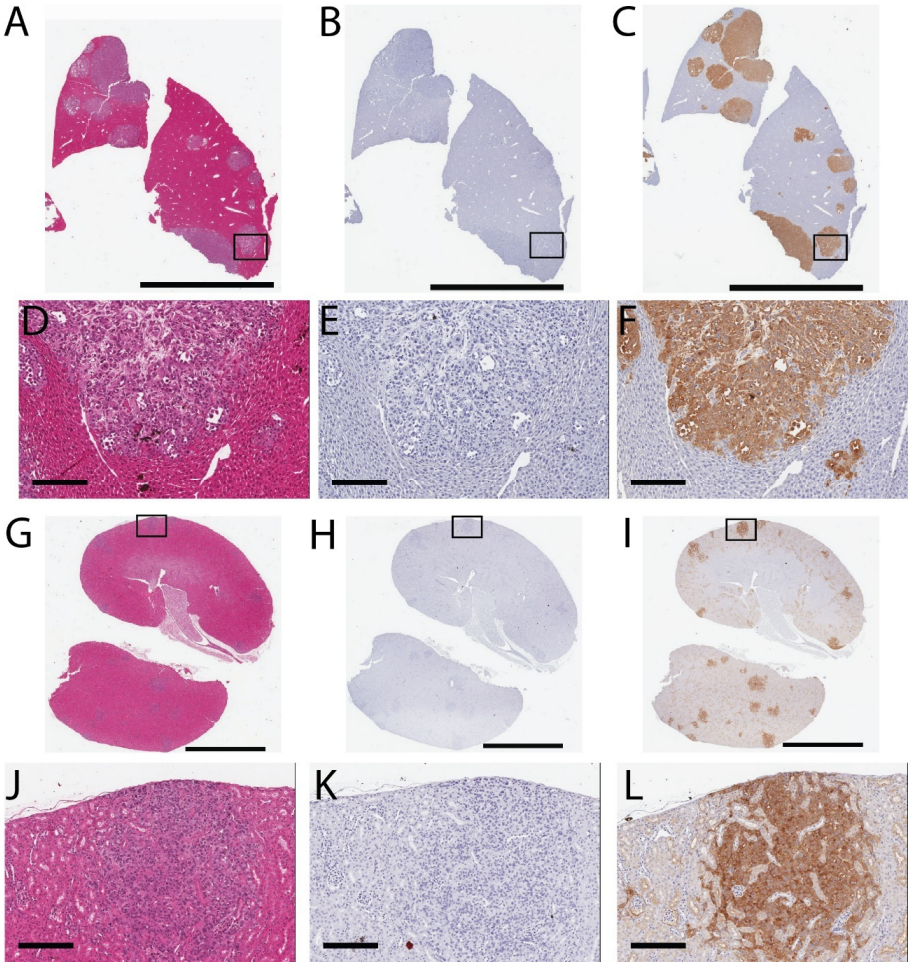

Figure 4. Immunohistochemistry confirmed the expression of PSMA in metastatic tumors and the cortex regions of mouse kidney. H&E staining (**A**,**D**,**G**,**J**), control staining without the 1° (anti-PSMA) Ab (**B**,**E**,**H**,**K**), and staining with anti-PSMA Ab (**C**,**F**,**I**,**L**). Scanned images of a whole section with 0.5× magnification (**A**–**C** and **G**–**I**, scale bar = 5 mm) and magnified images of boxed regions (**D**,**E**,**F**,**J**,**K**,**L**, scale bar = 200 μm) are shown.

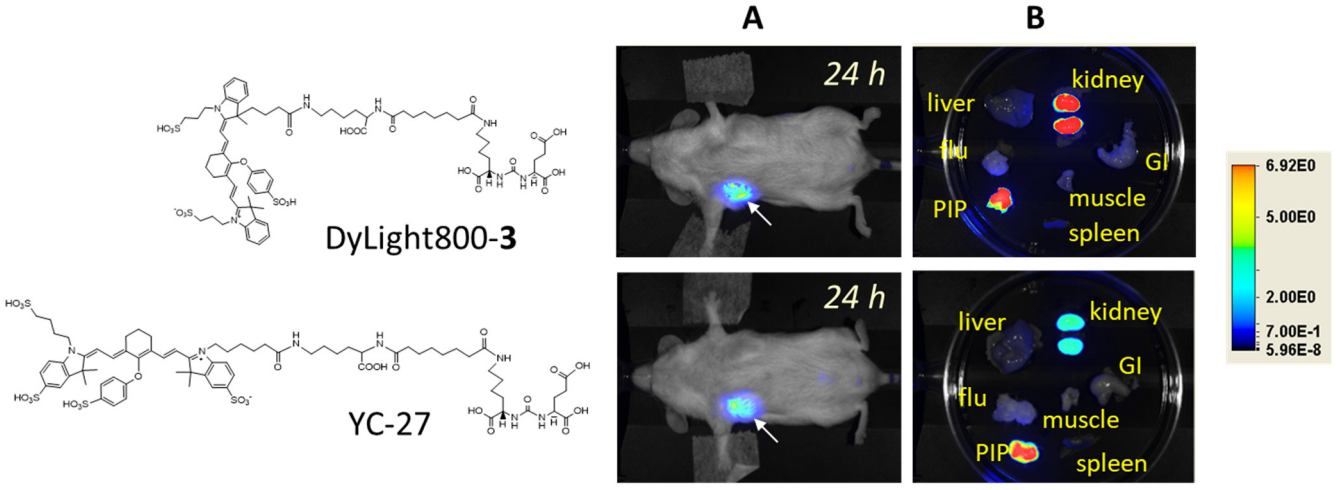

Figure 5. Head-to-head comparison of DyLight800-3 to YC-27. In each case, 1 nmol of agent was administered intravenously. Compounds provided comparable PSMA$^+$ PC3 PIP tumor (white arrows in column **A**) uptake at 24 h post-injection. At 24 h, animals were sacrificed and organs were removed and imaged (column **B**). Images are scaled to the same maximum value.

4. Discussion

FGS is increasingly employed for a variety of conditions, particularly in surgical oncology. As of today, Clinical trials.gov lists 53 active or recent studies involving FGS, with likely even more ongoing [30]. As with most imaging modalities, in order to be successful, high sensitivity and specificity are required for the NIR agent and the detection system. Here we have focused on optimization of what we have shown is a highly specific fluorescent platform for targeting PSMA [13–15]. We have done so in two ways: first, by replacing our initial fluorophore with DyLight800, due to its putatively superior quantum yields and photostability [23] and its ready availability. Second, we attempted to enhance the pharmacokinetics by altering the linker between the fluorophore and the PSMA-targeting moiety. We did so by altering the linker length, its overall degree of hydrophilicity and by affixing a bromobenzyl group to the ε-amino group of lysine, to which we also attached the fluorophore. We have previously shown that the *N*-bromobenzyl group in that position is capable of mitigating off-target tissue uptake [31].

Although these agents are suggested for use in enhancing surgery, which means that in the context of prostate cancer, only local images in the tumor margin or of local-regional lymph nodes would be obtained, since PSMA is expressed in the neovasculature of many other tumors, it is important to minimize uptake in other organs, such as the kidney. For example, we have previously shown that we can target clear cell renal cell carcinoma (ccRCC) to good effect with a positron-emitting version of our PSMA-targeting ureas, DCFPyL (piflufolostat F 18) [32–34], and could potentially use an optimized NIR version for surgical guidance in partial nephrectomy, for which non-targeted carbocyanine dyes have been leveraged [11]. In this instance, DyLight800-**10** may be the best agent among those synthesized here, as there is little renal uptake yet sufficient brightness to enable clear visualization of metastatic foci (Figure 2). That compound arguably demonstrates the highest signal-to-noise ratio. For prostate surgery, DyLight800-**3** or DyLight800-**3**–**4**, which contain an acid group in the linker, may be superior, as renal uptake would be of no consequence in the surgical field. Nevertheless, that high renal uptake may be indicative of other non-target binding, which would have to be evaluated further. In all, it appears that the presence of the longer linker and enhanced hydrophilicity, such as the introduction of an acid group or a polyethylene glycol (PEG) chain in the linker, improve pharmacokinetics. The presence of the *N*-bromobenzyl group increased $PSMA^+$ PIP tumor uptake. We hope that inclusion of the *N*-bromobenzyl substituent will also promote a decrease in salivary gland uptake, as it has for our corresponding radiotheranostics [31].

One strategy to improve the performance of PSMA-targeting agents for FGS is to use a fluorescent molecular rotor [35], which provides nearly instantaneous detection upon binding of PSMA. However, the clinical use and utility of such an agent may still be dictated by pharmacokinetics if administered intravenously. We must wait on the order of 12 to 24 h after administration for imaging in these preclinical models for clearance from non-target tissues. Others have developed NIR cancer detection agents that are merely sprayed onto the surgical site, further enhancing their convenience [36–38]. Whether those, or frankly any of these agents, actually improve outcomes measured by overall or progression-free survival remains to be determined in larger, prospective studies [5].

We undertook this study to optimize a PSMA-targeting NIR agent with respect to fluorophore and pharmacokinetics. Our qualitative, head-to-head comparison of DyLight800-**3** to YC-27 did not reveal a substantial difference in tumor uptake, although the latter had significantly lower renal uptake. The literature also provides little evidence for the superiority of DyLight800 over IRDye 800CW, and actually suggests the contrary in terms of quantum yield and brightness in certain in vitro assays [39,40]. Remaining, however, is the possibility that the issue of coupling a particular dye with a certain camera may further enhance sensitivity, while we used the Pearl Impulse Imager for our studies herein.

5. Conclusions

In conclusion, inclusion of an *N*-bromobenzyl substituent promoted increased PSMA$^+$ PIP tumor uptake, while a hydrophilic linker, particularly with the inclusion of PEG, may decrease nonspecific binding, particularly to the kidney, in this new series of PSMA-targeted NIR agents. Such modifications, perhaps coupled with what could be a truly superior flurophore [40], may render this latest generation of NIR probes even more suitable for FGS in prostate cancer, ccRCC or other PSMA-expressing tumors than existing agents.

Supplementary Materials: The following supporting information can be downloaded at: https://www.mdpi.com/article/10.3390/biom12030405/s1. Scheme S1: Reagent and conditions and corresponding synthetic detail.

Author Contributions: Conceptualization, Y.C., M.G.P., S.R.B. and R.C.M.; methodology, Y.C., I.M., A.L., S.C. and M.B.; resources, M.G.P.; writing—original draft preparation, Y.C., M.G.P. and R.C.M.; writing—review and editing, I.M., S.P.R., S.C., R.C.M. and M.G.P.; funding acquisition, M.G.P. All authors have read and agreed to the published version of the manuscript.

Funding: This research was funded by the NIH, CA134675 and EB024495.

Institutional Review Board Statement: The animal study protocol was approved by the Animal Care and Use Committee of The Johns Hopkins University (MO21M123; approved on 28 September 2021).

Informed Consent Statement: Not applicable.

Data Availability Statement: Not applicable.

Conflicts of Interest: Y.C., S.R.B., R.C.M. and M.G.P. have filed a patent application involving one or more of the compounds described herein. The funders had no role in the design of the study; in the collection, analyses, or interpretation of data; in the writing of the manuscript, or in the decision to publish the results.

References

1. Kularatne, S.A.; Thomas, M.; Myers, C.H.; Gagare, P.; Kanduluru, A.K.; Crian, C.J.; Cichocki, B.N.; Crain, C.J. Evaluation of Novel Prostate-Specific Membrane Antigen-Targeted Near-Infrared Imaging Agent for Fluorescence-Guided Surgery of Prostate Cancer. *Clin. Cancer Res.* **2018**, *25*, 177–187. [CrossRef] [PubMed]
2. Lwin, T.M.; Turner, M.A.; Amirfakhri, S.; Nishino, H.; Hoffman, R.M.; Bouvet, M. Fluorescence Molecular Targeting of Colon Cancer to Visualize the Invisible. *Cells* **2022**, *11*, 249. [CrossRef]
3. Nishio, N.; Berg, N.S.V.D.; Van Keulen, S.; Martin, B.A.; Fakurnejad, S.; Teraphongphom, N.; Chirita, S.U.; Oberhelman, N.J.; Lu, G.; Horton, C.; et al. Optical molecular imaging can differentiate metastatic from benign lymph nodes in head and neck cancer. *Nat. Commun.* **2019**, *10*, 1–10. [CrossRef] [PubMed]
4. Gibbs, S.L. Near infrared fluorescence for image-guided surgery. *Quant. Imaging Med. Surg.* **2012**, *2*, 177–187. [PubMed]
5. Thammineedi, S.R.; Saksena, A.R.; Nusrath, S.; Iyer, R.R.; Shukla, S.; Patnaik, S.C.; Reddy, R.P.; Boleneni, N.; Sharma, R.M.; Smith, L.; et al. Fluorescence-guided cancer surgery-A new paradigm. *J. Surg. Oncol.* **2021**, *123*, 1679–1698. [CrossRef] [PubMed]
6. Abrahimi, P.; McClure, T. Emerging Intraoperative Imaging Technologies in Urologic Oncology. *Urol. Clin. N. Am.* **2021**, *49*, 57–63. [CrossRef]
7. A Stern, L.; A Case, B.; Hackel, B.J. Alternative non-antibody protein scaffolds for molecular imaging of cancer. *Curr. Opin. Chem. Eng.* **2013**, *2*, 425–432. [CrossRef]
8. Fukuda, T.; Yokomizo, S.; Casa, S.; Monaco, H.; Manganiello, S.; Wang, H.; Lv, X.; Ulumben, A.D.; Yang, C.; Kang, M.W.; et al. Fast and Durable Intraoperative Near-infrared Imaging of Ovarian Cancer Using Ultrabright Squaraine Fluorophores. *Angew. Chem.* **2022**. [CrossRef]
9. Hingorani, D.V.; A Whitney, M.; Friedman, B.; Kwon, J.-K.; Crisp, J.L.; Xiong, Q.; Gross, L.; Kane, C.J.; Tsien, R.Y.; Nguyen, Q.T. Nerve-targeted probes for fluorescence-guided intraoperative imaging. *Theranostics* **2018**, *8*, 4226–4237. [CrossRef]
10. Wang, L.G.; Barth, C.W.; Kitts, C.H.; Mebrat, M.D.; Montaño, A.R.; House, B.J.; McCoy, M.E.; Antaris, A.L.; Galvis, S.N.; McDowall, I.; et al. Near-infrared nerve-binding fluorophores for buried nerve tissue imaging. *Sci. Transl. Med.* **2020**, *12*. [CrossRef]
11. Kaplan-Marans, E.; Fulla, J.; Tomer, N.; Bilal, K.; Palese, M. Indocyanine Green (ICG) in Urologic Surgery. *Urology* **2019**, *132*, 10–17. [CrossRef] [PubMed]
12. Van Dam, G.M.; Themelis, G.; Crane, L.M.; Harlaar, N.J.; Pleijhuis, R.G.; Kelder, W.; Sarantopoulos, A.; De Jong, J.S.; Arts, H.J.; Van Der Zee, A.G.; et al. Intraoperative tumor-specific fluorescence imaging in ovarian cancer by folate receptor-α targeting: First in-human results. *Nat. Med.* **2011**, *17*, 1315–1319. [CrossRef] [PubMed]
13. Chen, Y.; Dhara, S.; Banerjee, S.R.; Byun, Y.; Pullambhatla, M.; Mease, R.C.; Pomper, M.G. A low molecular weight PSMA-based fluorescent imaging agent for cancer. *Biochem. Biophys. Res. Commun.* **2009**, *390*, 624–629. [CrossRef] [PubMed]

14. Banerjee, S.R.; Pullambhatla, M.; Byun, Y.; Nimmagadda, S.; Foss, C.A.; Green, G.; Fox, J.J.; Lupold, S.E.; Mease, R.C.; Pomper, M.G. Sequential SPECT and Optical Imaging of Experimental Models of Prostate Cancer with a Dual Modality Inhibitor of the Prostate-Specific Membrane Antigen. *Angew. Chem. Int. Ed.* **2011**, *50*, 9167–9170. [CrossRef] [PubMed]
15. Chen, Y.; Pullambhatla, M.; Banerjee, S.R.; Byun, Y.; Stathis, M.; Rojas, C.; Slusher, B.S.; Mease, R.C.; Pomper, M.G. Synthesis and Biological Evaluation of Low Molecular Weight Fluorescent Imaging Agents for the Prostate-Specific Membrane Antigen. *Bioconjugate Chem.* **2012**, *23*, 2377–2385. [CrossRef]
16. Kelderhouse, L.E.; Chelvam, V.; Wayua, C.; Mahalingam, S.; Poh, S.; Kularatne, S.A.; Low, P.S. Development of Tumor-Targeted Near Infrared Probes for Fluorescence Guided Surgery. *Bioconjugate Chem.* **2013**, *24*, 1075–1080. [CrossRef]
17. Wang, X.; Huang, S.S.; Heston, W.D.; Guo, H.; Wang, B.-C.; Basilion, J.P. Development of Targeted Near-Infrared Imaging Agents for Prostate Cancer. *Mol. Cancer Ther.* **2014**, *13*, 2595–2606. [CrossRef]
18. Baranski, A.-C.; Schäfer, M.; Bauder-Wüst, U.; Roscher, M.; Schmidt, J.; Stenau, E.; Simpfendörfer, T.; Teber, D.; Maier-Hein, L.; Hadaschik, B.; et al. PSMA-11–Derived Dual-Labeled PSMA Inhibitors for Preoperative PET Imaging and Precise Fluorescence-Guided Surgery of Prostate Cancer. *J. Nucl. Med.* **2017**, *59*, 639–645. [CrossRef]
19. Liu, H.; Moy, P.; Kim, S.; Xia, Y.; Rajasekaran, A.; Navarro, V.; Knudsen, B.; Bander, N.H. Monoclonal antibodies to the extracellular domain of prostate-specific membrane antigen also react with tumor vascular endothelium. *Cancer Res.* **1997**, *57*, 3629–3634.
20. Chang, S.S.; E Reuter, V.; Heston, W.D.; Bander, N.H.; Grauer, L.S.; Gaudin, P.B. Five different anti-prostate-specific membrane antigen (PSMA) antibodies confirm PSMA expression in tumor-associated neovasculature. *Cancer Res.* **1999**, *59*, 3192–3198.
21. Neuman, B.P.; Eifler, J.B.; Castanares, M.; Chowdhury, W.; Chen, Y.; Mease, R.C.; Ma, R.; Mukherjee, A.; Lupold, S.E.; Pomper, M.G.; et al. Real-time, Near-Infrared Fluorescence Imaging with an Optimized Dye/Light Source/Camera Combination for Surgical Guidance of Prostate Cancer. *Clin. Cancer Res.* **2015**, *21*, 771–780. [CrossRef] [PubMed]
22. Zhang, H.K.; Chen, Y.; Kang, J.; Lisok, A.; Minn, I.; Pomper, M.G.; Boctor, E.M. Prostate-specific membrane antigen-targeted photoacoustic imaging of prostate cancer in vivo. *J. Biophotonics* **2018**, *11*, e201800021. [CrossRef] [PubMed]
23. ThermoFisher Scientific Product Guide. Available online: https://www.thermofisher.com/us/en/home/brands/thermo-scientific/pierce-protein-biology.html?cid=fl-ts-pierce (accessed on 22 February 2022).
24. Maresca, K.P.; Hillier, S.M.; Femia, F.J.; Keith, D.; Barone, C.; Joyal, J.L.; Zimmerman, C.N.; Kozikowski, A.P.; Barrett, J.A.; Eckelman, W.C.; et al. A Series of Halogenated Heterodimeric Inhibitors of Prostate Specific Membrane Antigen (PSMA) as Radiolabeled Probes for Targeting Prostate Cancer. *J. Med. Chem.* **2009**, *52*, 347–357. [CrossRef] [PubMed]
25. Tykvart, J.; Schimer, J.; Bařinková, J.; Pachl, P.; Poštová-Slavětínská, L.; Majer, P.; Konvalinka, J.; Šácha, P. Rational design of urea-based glutamate carboxypeptidase II (GCPII) inhibitors as versatile tools for specific drug targeting and delivery. *Bioorg. Med. Chem.* **2014**, *22*, 4099–4108. [CrossRef]
26. Chen, Y.; Pullambhatla, M.; Foss, C.A.; Byun, Y.; Nimmagadda, S.; Senthamizhchelvan, S.; Sgouros, G.; Mease, R.C.; Pomper, M.G. 2-(3-{1-Carboxy-5-[(6-[18F]fluoro-pyridine-3-carbonyl)-amino]-pentyl}-ureido)-pen tanedioic acid, [18F]DCFPyL, a PSMA-based PET imaging agent for prostate cancer. *Clin. Cancer Res. An Off. J. Am. Assoc. Cancer Res.* **2011**, *17*, 7645–7653. [CrossRef]
27. Cheng, Y.; Prusoff, W.H. Relationship between the inhibition constant (K1) and the concentration of inhibitor which causes 50 per cent inhibition (I50) of an enzymatic reaction. *Biochem. Pharmacol.* **1973**, *22*, 3099–3108.
28. Boinapally, S.; Ahn, H.-H.; Cheng, B.; Brummet, M.; Nam, H.; Gabrielson, K.L.; Banerjee, S.R.; Minn, I.; Pomper, M.G. A prostate-specific membrane antigen (PSMA)-targeted prodrug with a favorable in vivo toxicity profile. *Sci. Rep.* **2021**, *11*, 1–10. [CrossRef]
29. Rowe, S.P.; Drzezga, A.; Neumaier, B.; Dietlein, M.; Gorin, M.A.; Zalutsky, M.R.; Pomper, M.G. Prostate-Specific Membrane Antigen–Targeted Radiohalogenated PET and Therapeutic Agents for Prostate Cancer. *J. Nucl. Med.* **2016**, *57*, 90S–96S. [CrossRef]
30. Barth, C.W.; Gibbs, S.L. Fluorescence Image-Guided Surgery—A Perspective on Contrast Agent Development. *Proc. SPIE Int. Soc. Opt. Eng.* **2020**, *11222*, 112220J.
31. Banerjee, S.R.; Kumar, V.; Lisok, A.; Chen, J.; Minn, I.; Brummet, M.; Boinapally, S.; Cole, M.; Ngen, E.; Wharram, B.; et al. 177Lu-labeled low-molecular-weight agents for PSMA-targeted radiopharmaceutical therapy. *Eur. J. Pediatr.* **2019**, *46*, 2545–2557. [CrossRef]
32. Rowe, S.P.; Gorin, M.A.; Hammers, H.J.; Som Javadi, M.; Hawasli, H.; Szabo, Z.; Cho, S.Y.; Pomper, M.G.; Allaf, M.E. Imaging of metastatic clear cell renal cell carcinoma with PSMA-targeted (1)(8)F-DCFPyL PET/CT. *Ann. Nucl. Med.* **2015**, *29*, 877–882. [CrossRef] [PubMed]
33. Rowe, S.P.; Gorin, M.A.; Hammers, H.J.; Pomper, M.G.; Allaf, M.E.; Javadi, M.S. Detection of 18F-FDG PET/CT Occult Lesions With 18F-DCFPyL PET/CT in a Patient With Metastatic Renal Cell Carcinoma. *Clin. Nucl. Med.* **2016**, *41*, 83–85. [CrossRef] [PubMed]
34. Meyer, A.R.; Carducci, M.A.; Denmeade, S.R.; Markowski, M.C.; Pomper, M.G.; Pierorazio, P.M.; Allaf, M.E.; Rowe, S.P.; Gorin, M.A. Improved identification of patients with oligometastatic clear cell renal cell carcinoma with PSMA-targeted (18)F-DCFPyL PET/CT. *Ann. Nucl. Med.* **2019**, *33*, 617–623. [CrossRef]
35. Zhang, J.; Rakhimbekova, A.; Duan, X.; Yin, Q.; Foss, C.A.; Fan, Y.; Xu, Y.; Li, X.; Cai, X.; Kutil, Z.; et al. A prostate-specific membrane antigen activated molecular rotor for real-time fluorescence imaging. *Nat. Commun.* **2021**, *12*, 1–11. [CrossRef] [PubMed]
36. Hansen, S.J.; Olson, J.M. In Vivo Bio-imaging Using Chlorotoxin-based Conjugates. *Curr. Pharm. Des.* **2011**, *17*, 4362–4371.

37. Barth, C.W.; Gibbs, S.L. Direct Administration of Nerve-Specific Contrast to Improve Nerve Sparing Radical Prostatectomy. *Theranostics* **2017**, *7*, 573–593. [CrossRef]
38. Tung, C.-H.; Han, M.S.; Shen, Z.; Gray, B.D.; Pak, K.Y.; Wang, J. Near-Infrared Fluorogenic Spray for Rapid Tumor Sensing. *ACS Sens.* **2021**, *6*, 3657–3666. [CrossRef]
39. Tynan, C.J.; Clarke, D.; Coles, B.C.; Rolfe, D.; Martin-Fernandez, M.; Webb, S.E.D. Multicolour Single Molecule Imaging in Cells with Near Infra-Red Dyes. *PLoS ONE* **2012**, *7*, e36265. [CrossRef]
40. Schreiber, C.L.; Li, D.-H.; Smith, B.D. High-Performance Near-Infrared Fluorescent Secondary Antibodies for Immunofluorescence. *Anal. Chem.* **2021**, *93*, 3643–3651. [CrossRef]